Annales Geophysicae, 23, 3579–3590, 2005
SRef-ID: 1432-0576/ag/2005-23-3579

Annales Geophysicae

Tidal variations of O_2 Atmospheric and OH(6-2) airglow and temperature at mid-latitudes from SATI observations

M. J. López-González[1], E. Rodríguez[1], G. G. Shepherd[2], S. Sargoytchev[2], M. G. Shepherd[2], V. M. Aushev[3], S. Brown[2], M. García-Comas[1], and R. H. Wiens[4]

[1]Instituto de Astrofísica de Andalucía, CSIC, P.O. Box 3004, E-18080 Granada, Spain
[2]Centre for Research in Earth and Space Science, York University, 4700 Keele St., Toronto, Ontario M3J 1P3, Canada
[3]Institute of Ionosphere, Ministry of Education and Science, Almaty, 480020, Kazakhstan
[4]Department of Physics, University of Asmara, Eritrea, N. E. Africa

Received: 16 September 2005 – Revised: 18 October 2005 – Accepted: 27 October 2005 – Published: 23 December 2005

Abstract. Airglow observations with a Spectral Airglow Temperature Imager (SATI), installed at the Sierra Nevada Observatory (37.06° N, 3.38° W) at 2900-m height, have been used to investigate the presence of tidal variations at mid-latitudes in the mesosphere/lower thermosphere region. Diurnal variations of the column emission rate and vertically averaged temperature of the O_2 Atmospheric (0-1) band and of the OH Meinel (6-2) band from 5 years (1998–2003) of observations have been analysed. From these observations a clear tidal variation of both emission rates and rotational temperatures is inferred. It is found that the amplitude of the daily variation for both emission rates and temperatures is greater from late autumn to spring than during summer. The amplitude decreases by more than a factor of two during summer and early autumn with respect to the amplitude in the winter-spring months. Although the tidal modulations are preferentially semidiurnal in both rotational temperatures and emission rates during the whole year, during early spring the tidal modulations seem to be more consistent with a diurnal modulation in both rotational temperatures and emission rates. Moreover, the OH emission rate from late autumn to early winter has a pattern suggesting both diurnal and semidiurnal tidal modulations.

Keywords. Atmospheric composition and structure (Airglow and aurora; pressure density and temperature; instruments and techniques)

1 Introduction

Airglow emissions have been used to study the chemical and dynamical behaviour of the atmosphere in those regions where the emission takes place. Atmospheric tides are the global response of the atmosphere to the periodic forcing of solar heating. The influence of the atmospheric tides on the airglow emissions has been studied since 1970 (e.g. Wiens and Weill, 1973; Petitdidier and Teitelbaum, 1977; Takahashi et al., 1977). The tides present periodicities equal to the solar day and its harmonics, and propagate westward following the motion of the Sun (e.g. Chapman and Lindzen, 1970).

There is an enormous body of ground-based observations of the mesosphere and lower thermosphere by the global radar network (e.g. Jacobi et al., 1999; Pancheva et al., 2000, 2002; Riggin et al., 2003; Forbes et al., 2004; Manson et al., 2004; Portnyagin et al., 2004) that have been used to study the tidal behaviour of the atmospheric winds. Studies of the influences of atmospheric tides on airglow emission and temperature using long-term, ground-based observations (e.g. Wiens and Weill, 1973; Petitdidier and Teitelbaum, 1977; Scheer and Reisin, 1990; Reisin and Scheer, 1996; Takahashi et al., 1998; Choi et al., 1998) and satellite airglow observations (Abreu and Yee, 1989; Burrage et al., 1994; Shepherd et al., 1995, 1998) have shown a large variation in diurnal behaviour of the airglow emission rates as a function of the year and of the latitude.

Simultaneous satellite observations of emission rates, temperatures and winds performed with the High Resolution Doppler Imager (HRDI) and Wind Imaging Interferometer (WINDII), both on board the UARS satellite, have been used to study the tidal variations in airglow emission rates and winds (Burrage et al., 1994; Shepherd et al., 1995, 1998; Shepherd et al., 2004a).

Here, we analysed the tidal variation found from long-term, ground-based airglow observations at 37.06° N latitude. These observations have been made by a Spectral Airglow Temperature Imager (SATI) instrument placed at the Sierra Nevada Observatory. This instrument is able to

Correspondence to: M. J. López-González
(mariajose@iaa.es)

measure the column emission rate and the vertically averaged rotational temperature of both the O_2 Atmospheric (0-1) band, and the OH Meinel (6-2) band, using the technique of interference filter spectral imaging with a cooled CCD detector (Wiens et al., 1997). The data analysed cover a period from 1998 to 2003. Tidal variations of the temperature and airglow emission rates of the O_2 Atmospheric (0-1) band and the OH Meinel (6-2) band are presented and compared with previous results. It is shown that the diurnal variation of the emission rates and temperatures has a seasonal dependence. The amplitudes of the variations observed during late autumn to spring are greater by more than a factor of two than those observed during the rest of the year.

2 Observations

SATI is installed at the Sierra Nevada Observatory (37.06° N, 3.38° W), Granada, Spain, at 2900-m height. It has been in continuous operation since October 1998. SATI is a spatial and spectral imaging Fabry-Perot spectrometer in which the etalon is a narrow band interference filter and the detector is a CCD camera. The SATI instrumental concept and optical configuration was originally developed as the Mesopause Oxygen Rotational Temperature Imager (MORTI) instrument (Wiens et al., 1991). The new adaptation as SATI is described in detail by Sargoytchev et al. (2004). The instrument uses two interference filters, one centred at 867.689 nm (in the spectral region of the O_2 Atmospheric (0-1) band) and the second one centred at 836.813 nm (in the spectral region of the OH Meinel (6-2) band). Its field of view is an annulus of 30° average radius and 7.1° angular width, centered on the zenith. Thus, an annulus of average radius of 55 km and 16 km width at 95 km (or an average radius of 49 km and 14 km width at 85 km) is observed in the sky.

The images are disks where the polar angle dimension corresponds to the azimuth of the ring of the sky observed, while the radial distribution of the images contains the spectral distribution, from which the rotational temperature is inferred. The method of SATI image reduction and temperature and emission rate determination was described in detail by Wiens et al. (1991) for the O_2 Atmospheric system, and by López-González et al. (2004) for the OH(6-2) Meinel band.

In this work the images obtained from SATI are analysed as a whole, obtaining an average of the rotational temperature and emission rate of the airglow band from the whole sky ring.

The seasonal variation in rotational temperatures and airglow emission rates measured with the SATI instrument during the period of October 1998 to March 2002 have been analysed and presented by López-González et al. (2004). In the current study new data from March 2002 to May 2003 have been added to the earlier data set and are analysed, in order to derive the tidal variations present in both rotational temperatures and emission rates. The OH temperatures deduced from the Q-branch have been corrected from the error introduced by using Q-branch theoretical Einstein coefficients (see Pendleton and Taylor, 2002).

Table 1 shows the number of days and hours of observation used in the study, in each month from October 1998 to May 2003. Table 1 also shows the total number of days and hours per month. We have used all the data corresponding to good observing conditions, even data corresponding to short days of observations, with the aim of obtaining the largest amount of data.

There are months, such as January 1999, when only two short nights of data are available, and the nocturnal variation of this month covers only one-third of the night compared with January data of other years. However, although only one-third of the night was covered, a strong correlation existed with the nocturnal variation during this one-third of the night and that obtained during the January nights of other years.

López-González et al. (2004) have shown that rotational temperatures and emission rates have a marked short-term variability together with a clear seasonal variation. Tables 2 and 3 show the mean rotational temperatures ($\overline{T_{O_2}}$ and $\overline{T_{OH}}$) and emission rates ($\overline{E_{O_2}}$ and $\overline{E_{OH}}$) for each month of the year due to the seasonal variation of these parameters found in SATI data. In Tables 2 and 3 are also listed other quantities that will be discussed in the following section: the absolute amplitudes of the temperature and emission rate variations (ΔT_{O_2}, ΔT_{OH}, ΔE_{O_2} and ΔE_{OH}), the relative temperature and emission rate amplitudes, ($\frac{\Delta T_{O_2}}{\overline{T_{O_2}}}$, $\frac{\Delta T_{OH}}{\overline{T_{OH}}}$, $\frac{\Delta E_{O_2}}{\overline{E_{O_2}}}$ and $\frac{\Delta E_{OH}}{\overline{E_{OH}}}$), the amplitudes and phases of the Krassovsky ratio ($|\eta|$,ϕ) and the vertical wavelengths (λ_z) for the propagation of the tidal modulations found from both emissions.

Here our interest is to determine the tidal variations and the seasonal dependences of these tidal variations. First of all, we subtracted the annual and semiannual seasonal variations in the rotational temperature and emission rates of both OH and O_2 emissions (see Tables 2 and 3). Here we employ the residual temperatures and emission rates after removing the seasonal dependences.

For the systematic organization of the data we average these residual rotational temperatures and emission rates from each night over 30-min intervals, centered on the hours and half hours. Thus, an averaged nighttime variation is obtained for each night of available data, for every night of the month. This reduces short-period variations but does not affect tidal components. By averaging the values obtained at the same local time over one month, we obtain the diurnal variation for each month of available observations in each year of SATI observations. A "mean" monthly diurnal variation is then derived by averaging the monthly diurnal variations over the 5-year period.

3 Results

The averaged diurnal variations, for each month, from 1998 to 2003, together with the "mean" diurnal variation, are

Table 1. Airglow observations.

	1998		1999		2000		2001		2002		2003		Total	
Month	nights	hours	nights	hours	nights	hours	nights	hours	nights	hours	nights	hours	nights	hours
January			2	7	6	23	5	27	12	90			25	151
February			17	94	13	150	3	20	16	109	8	69	57	373
March			15	93	14	122	19	119	11	62			59	396
April			9	69	9	58	11	63					29	193
May			5	36			12	80			12	67	29	183
June			5	34			8	36	21	84			38	154
July			15	81	4	17	5	24	23	85			47	207
August			5	20	18	105	6	30	22	103			51	258
September					12	67	12	85	19	100			43	252
October	22	174	6	36	16	112	18	90	11	43			73	455
November	23	172	9	88					18	98			50	358
December	11	86	11	89			6	26	19	91			47	292

Table 2. Summary of wave parameters from OH layer. Solutions obtained from amplitudes smaller than 3 K are listed in bold.

Month	$\overline{E_{\mathrm{OH}}}$(R)	ΔE_{OH} (R)	$\frac{\Delta E_{\mathrm{OH}}}{\overline{E_{\mathrm{OH}}}}$	$\overline{T_{\mathrm{OH}}}$(K)	ΔT_{OH} (K)	$\frac{\Delta T_{\mathrm{OH}}}{\overline{T_{\mathrm{OH}}}}$	$\lvert\eta\rvert$	ϕ (degree)	λ_z (km)
January	793	171.2	0.216	211	4.8	0.0228	9.5	−77.9	−14.3
February	692	178.3	0.258	208	6.5	0.0314	8.2	−70.7	−17.0
March	637	188.7	0.296	205	5.4	0.0265	11.2	−88.7	−11.8
April	652	160.9	0.247	199	2.6	0.0129	**19.1**	**−158.9**	**−19.1**
May	690	151.8	0.220	192	1.2	0.0060	**36.7**	**+138.4**	**+5.4**
June	686	101.0	0.147	186	–	–	–	–	–
July	672	93.5	0.139	185	–	–	–	–	–
August	572	106.7	0.187	191	0.8	0.0039	**47.9**	**−142.9**	**−4.6**
September	591	104.3	0.176	200	2.2	0.0110	**16.0**	**+64.4**	**+9.1**
October	694	94.4	0.136	209	1.6	0.0074	**18.4**	**−115.4**	**−8.0**
November	813	166.0	0.204	213	6.0	0.0282	7.2	−112.1	−19.7
December	862	142.7	0.165	214	5.2	0.0243	6.8	−99.5	−19.7

Table 3. Summary of wave parameters from O_2 layer. Solutions obtained from amplitudes smaller than 3 K are listed in bold.

Month	$\overline{E_{\mathrm{O_2}}}$(R)	$\Delta E_{\mathrm{O_2}}$ (R)	$\frac{\Delta E_{\mathrm{O_2}}}{\overline{E_{\mathrm{O_2}}}}$	$\overline{T_{\mathrm{O_2}}}$(K)	$\Delta T_{\mathrm{O_2}}$ (K)	$\frac{\Delta T_{\mathrm{O_2}}}{\overline{T_{\mathrm{O_2}}}}$	$\lvert\eta\rvert$	ϕ (degree)	λ_z (km)
January	364	120.8	0.332	193	10.9	0.0565	5.9	−33.5	−40.7
February	323	128.3	0.397	192	10.4	0.0541	7.3	−41.6	−27.1
March	341	116.9	0.343	193	6.7	0.0349	9.8	−46.4	−18.5
April	384	43.6	0.114	192	5.0	0.0261	4.4	−63.7	−33.7
May	395	35.7	0.090	187	5.6	0.0300	3.0	−48.9	−58.4
June	358	54.9	0.153	180	5.2	0.0287	5.5	−36.3	−40.8
July	313	45.6	0.146	178	3.9	0.0217	6.7	−21.9	−52.6
August	313	30.1	0.096	182	5.5	0.0303	3.2	−38.4	−111.8
September	376	38.6	0.103	191	4.0	0.0212	4.9	−38.6	−43.8
October	458	38.2	0.083	198	2.0	0.0099	**8.4**	**+50.8**	**+20.3**
November	492	156.1	0.317	201	11.3	0.0563	5.6	−33.9	−42.0
December	453	151.3	0.334	198	11.1	0.0559	6.0	−35.7	−37.8

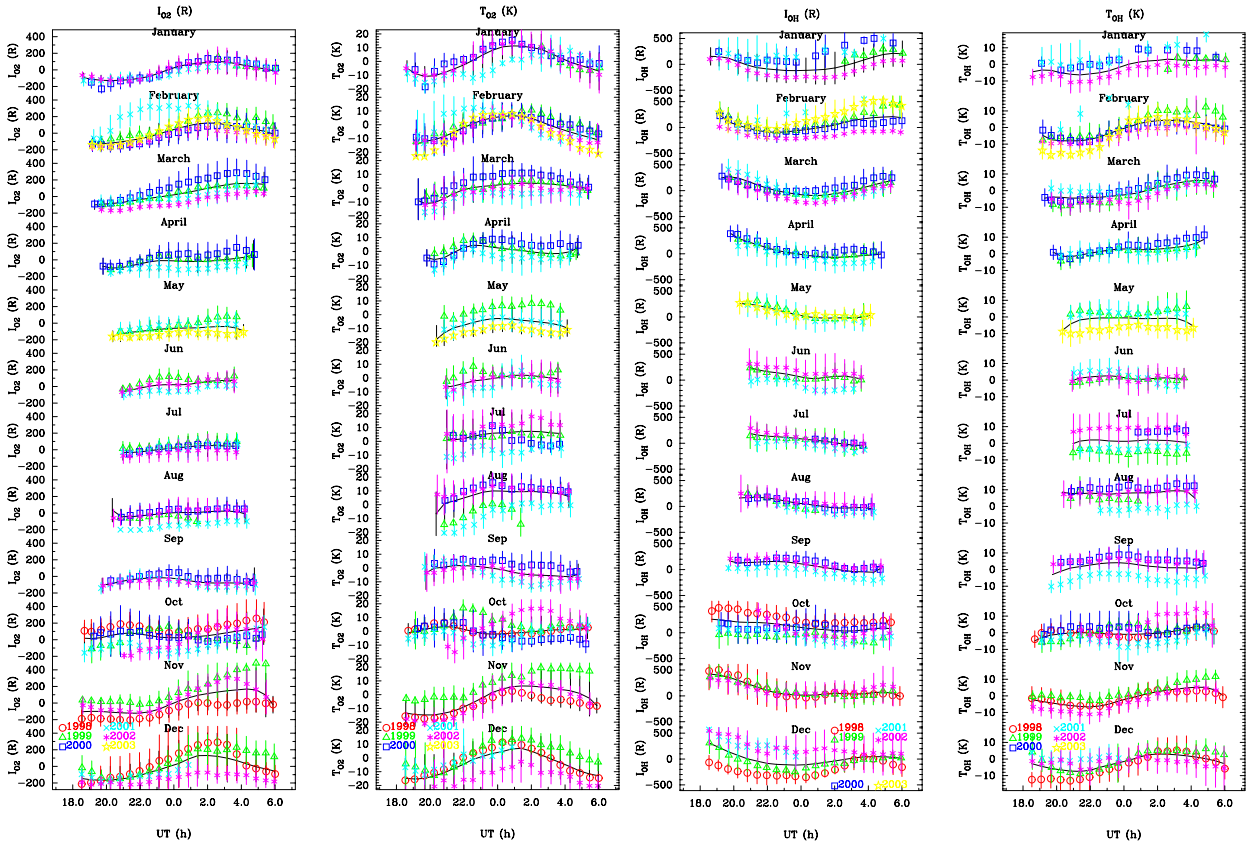

Fig. 1. Emission rates and rotational temperatures after removing seasonal annual and semiannual variations. Red circles: 1998. Green triangles: 1999. Blue squares: 2000. Blue crosses: 2001. Pink asterisks: 2002. Yellow stars: 2003. Solid line: Mean monthly night variations.

plotted in Fig. 1. The results show that the diurnal pattern obtained for each month is very similar for the different years from 1998 to 2003, and so is the "mean" monthly diurnal variation averaged over all years. Thus, it is easy to see for all years, for example, that in January the O_2 emission rate begins to decrease, creating minima at about four hours before midnight, and then increases until maxima are formed about 2 or 3 h after midnight (even in January 1999, where less than 4 h of data are available, these data follow the same behaviour as the other January months). However, the OH emission rate begins to decrease, creating minimum values at midnight. On the other hand, O_2 rotational temperature (T_{O_2}) and OH rotational temperature (T_{OH}) have a similar pattern of variation to that of the O_2 emission rate, although the maximum values of the O_2 temperature are reached about two hours earlier. Different patterns of diurnal variations are found for each month of the year. The presence of a modulation with a time period of 12 h is clearly seen in the winter months in both rotational temperatures and O_2 emission rates (see Fig. 1).

The number of night hours of each month goes from around 7 h in June to about 12 h of night coverage in December. Crary and Forbes (1983) showed that it is possible to extract semidiurnal and diurnal tides using data of limited temporal length, if these are closely spaced and averaged over several nights. Since we are working with data measured in exposure times of 2 min, averaged over the different days of each month during 5 years, we can have some qualitative information about the relative significance of the tidal components, but this nocturnal coverage is insufficient for finding a unique mathematical solution of the different tidal components (see Wiens et al., 1995).

The amplitudes and phases for diurnal and/or semidiurnal modulations that best fit the data have been obtained using a least-squares procedure, by using a diurnal or a semidiurnal variation, or simultaneously both variations. The solution with a least standard deviation after the fitting was adopted as the most probable result, although as was noted before, due to the short fraction of the day covered by the data, we cannot claim its mathematical uniqueness. Although a solution as a combination of a diurnal plus a semidiurnal tide has a least standard deviation, this solution, in almost all cases, is not reliable and produces large diurnal and semidiurnal amplitudes and different phases than those obtained when just one modulation is considered as the solution. We have considered only one case, in December for the OH emission rate,

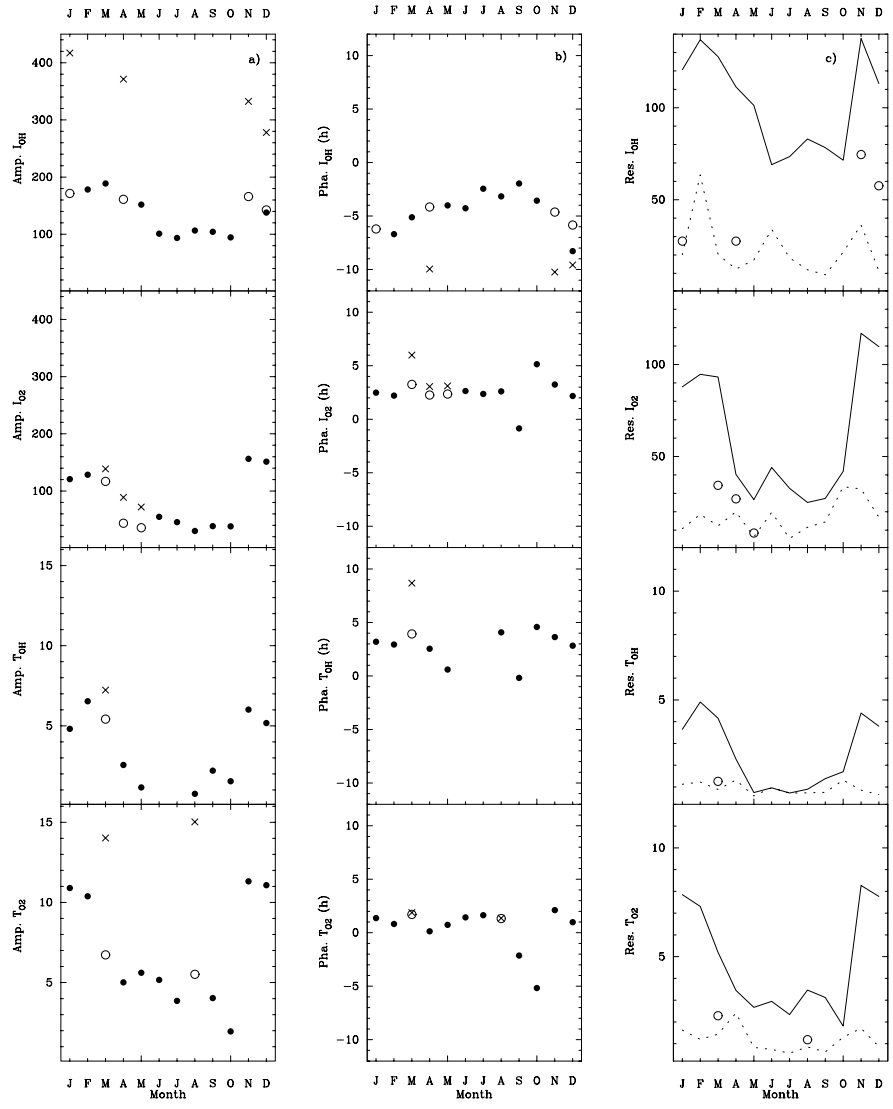

Fig. 2. (a) Relative amplitudes observed. **(b)** Phase of maxima. Crosses: diurnal tide. Black circles: semidiurnal tide. White circles: less probable semidiurnal fitting. **(c)** Residuals. Solid line: before fitting. Dashed line: after the fitting. White circles: after the fitting with a less probable semidiurnal fitting.

in which the solution could be a combination of the diurnal and the semidiurnal modulation (because the amplitudes and phases of the diurnal and semidiurnal component do not change much when a combination of both tidal components is considered). The amplitudes and phases, as well as the standard deviation of the data, with respect to their mean value before and after the best fitting, are listed in Table 4 and plotted in Fig. 2.

The diurnal variation of the OH emission rate found throughout the night is similar to that reported from WINDII OH emissions measurements at mid-latitudes (Zhang and Shepherd, 1999; Zhang et al., 2001).

The diurnal tide seems to be consistent with our observations in early spring from both emission rates and temperatures, while the semidiurnal tide is predominant for the rest of the year in the O_2 emission rate and both temperatures. This seasonal dependence is in agreement with the seasonal dependence found by Wiens et al. (1995) from ground-based measurements of the O_2 emission rate and temperature with the MORTI instrument at 42° N. They found tidal variations for O_2 and T_{O_2} to be semidiurnal in winter, diurnal in March and not clearly diurnal or semidiurnal in April. Shepherd et al. (1995, 1998) also reported a semidiurnal tide at mid-latitude in the Northern Hemisphere during winter solstice, determined from the WINDII O(^{1}S) green line emission rates, while at equinoxes the modulation changed to diurnal. This agrees with the behaviour found from SATI data for the O_2 emission rate, and both rotational temperatures, although from our data the semidiurnal modulations also remains in autumn.

Burrage et al. (1995) employed HRDI data and found that the horizontal wind at 95 km is dominated by the semidiurnal

Table 4. Tidal amplitudes and phases that best fit the data (semidiurnal tidal solutions with large standard deviations in bold).

			T_{O_2}			
	diurnal		semidiurnal			
Month	A_1 (K)	ϕ_1 (h)	A_2 (K)	ϕ_2 (h)	res_i	res_f
January			10.90	1.370	7.85	1.63
February			10.38	0.820	7.31	1.20
March	14.02	1.890			5.20	1.44
March			**6.730**	**1.710**	**5.20**	**2.29**
April			5.01	0.136	3.45	2.41
May			5.61	0.738	2.67	0.83
June			5.16	1.413	2.95	0.74
July			3.86	1.633	2.34	0.56
August	15.03	1.355			3.46	0.85
August			**5.512**	**1.322**	**3.46**	**1.18**
September			4.04	−2.134	3.12	0.63
October			1.96	6.824	1.81	1.29
November			11.32	2.114	8.27	1.71
December			11.07	0.981	7.77	0.86
			T_{OH}			
January			4.81	3.194	3.65	1.12
February			6.54	2.946	4.90	1.22
March	7.23	8.685			4.16	0.88
March			**5.42**	**3.925**	**4.16**	**1.26**
April			2.56	2.551	2.28	1.32
May			1.15	0.601	0.75	0.59
June					0.96	0.96
July					0.72	0.72
August			0.75	4.075	0.90	0.73
September			2.20	−0.186	1.38	0.75
October			1.55	4.584	1.70	1.32
November			6.01	3.637	4.40	0.85
December			5.18	2.831	3.79	0.65
			I_{O_2}			
January			120.80	2.486	87.91	10.81
February			128.31	2.208	94.66	18.55
March	138.72	6.000			93.18	12.33
March			**116.85**	**3.258**	**93.18**	**34.33**
April	88.81	3.055			40.26	19.98
April			**43.63**	**2.258**	**40.26**	**27.05**
May	71.89	3.112			26.57	6.33
May			**35.74**	**2.367**	**26.57**	**8.40**
June			54.86	2.640	44.03	19.66
July			45.61	2.362	32.71	5.48
August			30.06	2.600	25.03	11.54
September			38.58	−0.848	27.20	14.47
October			38.24	5.130	41.97	33.60
November			156.11	3.242	116.93	32.36
December			151.29	2.173	109.72	16.97
			I_{OH}			
January	417.11	−12.201			120.69	20.17
January			**171.24**	**−6.211**	**120.69**	**27.54**
February			178.30	−6.696	136.97	63.53
March			188.70	−5.118	127.77	20.29
April	371.22	−9.559			111.34	12.35
April			**160.94**	**−4.154**	**111.34**	**27.53**
May			151.83	−4.011	101.27	17.30
June			101.03	−4.274	69.09	33.90
July			93.47	−2.448	73.41	18.47
August			106.71	−3.164	83.06	11.98
September			104.27	−1.961	78.36	9.23
October			94.43	−3.571	71.53	21.52
November	332.28	−10.241			137.63	36.35
November			**165.98**	**−4.628**	**137.63**	**74.60**
December	277.93	−9.585	137.91	−8.283	113.16	11.26
December			**142.66**	**−5.854**	**113.16**	**57.60**

tide at latitudes greater than ±40°. They found that this semidiurnal variation is larger in winter than in summer. They also found that the semidiurnal tide at 95 km is less evident at the March/April equinox compared to the summer and winter solstices, and even compared to the September equinox. This behaviour is the same as that found here for our O_2 emission rate and both rotational temperatures obtained from SATI data. The semidiurnal variation even disappears in spring when it becomes predominantly diurnal. In general, the amplitude of the semidiurnal tide, obtained from SATI observations, is greater in winter and autumn than in summer.

The diurnal behaviour of the OH emission rate deduced from SATI data is rather different from that of the O_2 emission rates. The diurnal tide for the OH emission rate is not only predominant in spring, as for the O_2 emission rate and both temperatures, but also seems to be present from late autumn to early winter. Although this tidal behaviour of the OH emission rate during winter suggests that the diurnal type of modulation is present, the conclusion has to be considered with caution, because, as can be seen in Table 4, the standard deviation after the fitting is significantly smaller for December, while for January the standard deviation after the fitting is very close to that obtained by considering a semidiurnal tidal modulation in fitting of the data. During November the standard deviation after the fitting is greater than the standard deviation obtained after the fitting during the other months of the year. This can indicate that during November other tidal modulations which are not considered here can be present in the nocturnal variation of the OH emission. Bearing in mind that the great variability detected this month could be responsible for this tidal behaviour, this OH tidal behaviour may also indicate that the tidal response of the combination of the tidal responses of the different chemical species involved in the chemistry of vibrationally excited OH, mainly atomic hydrogen and ozone, at the altitude of the OH emission peak, is not identical to the combination of the tidal responses of the chemical species involved in the $O_2(b)$ chemistry, primarily atomic oxygen, at the $O_2(b)$ emission peak. Then, even if the tidal modulations were identical, the amplitudes and the phases of these modulations would be different at different altitudes (see López-González et al., 1996, for a model response of the neutral atmosphere to a forced wave modulation). The rotational temperatures deduced from both atmospheric emissions have a similar pattern of variation, indicating that, although at different altitudes the tidal pattern of the modulations is the same, the amplitude of the tidal variation is, in general, smaller for the OH temperatures than for the O_2 temperatures.

The amplitudes and phases of the most probable numerical solution obtained (the one that best fits the data) are plotted in Fig. 2. However, in the cases where the most probable numerical solution is the diurnal, we have plotted these amplitudes and phases together with those obtained with a possible semidiurnal modulation (also listed in Table 4 with bold characters). In these cases the standard deviations of the semidiurnal modulation are a little greater than those obtained with

the diurnal modulation, but in these cases, while these differences are not very big and might be indicative that the diurnal solution could be more appropriate, the numerical solution has to be considered with caution.

In the following subsections, for the sake of comparison, we will use the amplitudes and the phases obtained, considering as solution the semidiurnal tidal modulation, even in those cases where the semidiurnal tidal solution is not the one with least standard deviation after the fitting of the data.

3.1 Amplitudes

Figure 2a shows that from late autumn to spring the amplitudes of the modulation of both rotational temperatures and emission rates are greater than those during summer. In early spring this modulation seems to be preferentially diurnal in both rotational temperatures and emission rates, while during the rest of the year this modulation is clearly semidiurnal in both temperatures and O_2 emission rates, although for the OH emission rate the semidiurnal modulation seems to be present along with a diurnal modulation from late autumn to early winter.

The amplitudes for the nightly variations of both emission rates and rotational temperatures from November to March were found to be greater than in the rest of the year. Other measurements at mid-latitudes have already yielded a greater amplitude variation in winter (see, e.g. Wiens and Weill, 1973, for OH emission rates at 44° N and Choi et al., 1998, for OH temperatures and emission rates at 42° N).

Shepherd and Fricke-Begemann (2004) examined the temperature variability in the upper mesosphere, due to migrating tides, by combining daytime temperature observations of the WINDII satellite experiment with nighttime ground-based potassium lidar measurements at 28° N. They reported a semidiurnal tidal amplitude of 9 K in November and 4 K in May. From our measurements for 37.06° N we find an even smaller amplitude in the two data periods, but a larger difference between them, with amplitudes for the semidiurnal tide of 6 K in November and 1 K in May.

From our data we found a semidiurnal tide to be more consistent with our November to February observations. The amplitude of the tidal modulation is maximum during these months, about 10–11 K for T_{O_2} and about 5–6 K for T_{OH}. In April the amplitude decreases, reaching an amplitude of 5.6 K for T_{O_2} and 1.1 K for T_{OH} in May. The amplitudes of the semidiurnal modulation also decrease in early summer, although not as much, and remain small in the summer months and early autumn, September–October, until November, when a sharp increase in the tidal amplitudes is detected in both emission rates and rotational temperatures. During summer in the T_{OH} data, neither a diurnal nor semidiurnal tidal modulation is clearly detected (June–July). The standard deviation of the T_{OH} data before and after the fitting are nearly the same from May to August, while for the rest of the year the standard deviation after the fitting is smaller than the standard deviation of the data before the fitting, by a factor of about 2. So the results obtained from May to August for the OH temperatures have to be considered with caution.

The absolute amplitudes of the O_2 emission rate and of both temperatures are larger by more than a factor of two, and by a somewhat smaller ratio for the OH emission rate variation, from November to February, as compared with the summer months (see Tables 2 and 3).

3.2 Amplitude growth factor

Without energy dissipation the amplitude of a nonevanescent wave with upward propagation would grow from the OH to the O_2 emission layer, as the atmospheric density decreases. The observed relative amplitude growth factor in the rotational temperature (defined as the ratio of the relative amplitude of the temperature in the O_2 and OH layers) has been calculated using the amplitude obtained for the semidiurnal tidal solution in all cases, for the sake of comparison (see Table 5). Liu and Swenson (2003) predict for saturated waves (those whose amplitude does not change with the altitude) a relative amplitude growth factor that goes from 2.2 to 1.0 for waves of vertical wavelength, λ_z, from 15 km to 50 km (similarly, values from 2.0 to 1.3 for the growth factor of the relative amplitudes of the O_2 and OH emission rates are reported for waves with the same vertical wavelength). This ratio is larger for nonevanescent waves (those whose amplitude increases with the altitude) and smaller for waves with larger attenuation. Here we obtain values that are in the range of values predicted by the model of Liu and Swenson (2003) for nonevanescent waves of vertical wavelength, as detected in the semidiurnal tidal modulations of OH and O_2 temperatures (Sect. 3.4). The observed amplitude temperature growth factors are greater during May and August but, due to the undetectability or small amplitude variations detected in the OH rotational temperatures from May to August, the growth temperature factor during these months is affected by large uncertainties, and there is no confidence in the growth factor obtained. Reisin and Scheer (1996) have reported values from 0.9 to 1.7 obtained from observations at mid-latitudes in individual nights, at different times of the year, which are smaller than those obtained here, indicating a stronger wave attenuation in their data on individual nights than those obtained from our monthly mean nocturnal variations.

3.3 Phases

The phases of maxima obtained for both temperatures and emission rates are plotted in Fig. 2b. To make feasible the comparison of the phases we have plotted the phases of maximum, considering in all cases a semidiurnal modulation as the solution (see Fig. 3). The phase in T_{O_2} temperature is quite stable during the year with maxima in temperature at about one hour after midnight (see Figs. 3a and c). Major changes in the phase of T_{O_2} occur in September and October. Also, the phase in the O_2 emission rate is quite stable during the whole year, with maxima about two to three hours

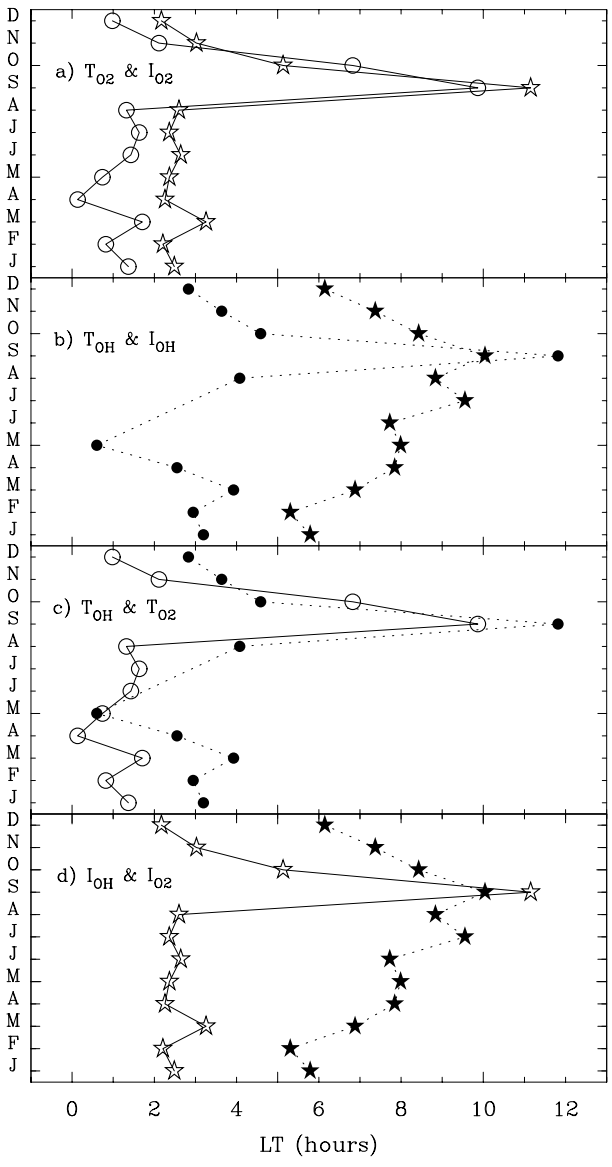

Fig. 3. Phases of maximum. **(a)** T_{O_2} and I_{O_2}. **(b)** T_{OH} and I_{OH}. **(c)** T_{O_2} and T_{OH}. **(d)** I_{OH} and I_{O_2}. White circle (solid line): T_{O_2}. White star (solid line): I_{O_2}. Black circle (dashed line): T_{OH}. Black star (dashed line): I_{OH}.

after midnight. There are exceptions to this stable phase behaviour, as in the O_2 temperature, for the months of September and October. It can be seen that the maxima in the O_2 emission rates occur about one or two hours later than those in T_{O_2}. So, O_2 temperatures lead the O_2 emission rates. This pattern is maintained for almost the whole year.

The time of the OH temperature maximum is also relatively stable during the year, with a maximum in OH rotational temperature at about a mean value of 4 h after midnight (see Figs. 3b and c). Again, large oscillations seem to be obtained at the times of the OH temperature maximum during September.

From Fig. 3c it is easy to see that the time of the OH temperature maximum is about 2 h later than the time of the maximum in O_2 temperature, with the exception of May and October, where the times of maximum OH temperature lead those of the O_2 temperature (see Fig. 3c). Thus, with those exceptions, and bearing in mind that the fitting of OH temperatures is difficult to detect from May to August (see Fig. 2b and Table 4), O_2 rotational temperatures lead OH temperatures for almost the entire year.

Figures 3b and d show that the maximum in the OH emission rate is always later than midnight. The maximum is about 6 h later than midnight from December to February (or 6 h before midnight). This means that OH emission rates reach minimum values close to midnight from December to February. From March to September the maximum values of the OH emission rates move toward later times, from 7 h later than midnight in March to 10 h later than midnight in September (or from 5 to 2 h before midnight, respectively). Then maximum values of OH emission rates move to earlier times in the night, as in winter months, from October to November.

The comparison of the times of maximum of the OH emission rates and temperatures shows that the OH emission rates reach a maximum about 3–4 h later than the maximum in OH temperatures from August to March, except in September, where the OH emission rate is maximum two hour before that of the OH temperature. During April and May the difference between the time of maximum OH emission rate and temperature increases, although it is during these months when it is difficult to find a semidiurnal modulation in OH temperatures.

The derived semidiurnal parameters from the SATI OH and O_2 temperature data have been compared with the semidiurnal parameters predicted by the Global Scale Wave Model (GSWM) (Hagan et al., 1999). The derived SATI phases of the temperature semidiurnal tide agree very well with those predicted by the GSWM at the respective heights. The OH semidiurnal phases of about 3–4 h local time are in excellent agreement with the GSWM phases predicted for the semidiurnal tide of about 15–16 h (or 3–4 h) solar local time, at 86.3 km height and 36 N latitude. Similarly, the O_2 semidiurnal tide phases are obtained at about 1–2 h local time, in agreement with the GSWM semidiurnal tide phases of 14–15 h (or 2–3 h) solar local time at 94.6 km height and 36 N. Further, the change in the OH phase derived from SATI for the month of September is in very good agreement with the GSWM model, while the change in the phase of the O_2 semidiurnal tide derived during September-October is predicted earlier in the model, from July to September. Although our derived SATI temperature semidiurnal tide amplitudes are somewhat larger than those predicted by the GSWM model, in general a good agreement is obtained between the SATI derived semidiurnal tide parameters and the parameters predicted by the GSWM model.

3.4 Vertical wavelengths

The Krassovsky ratio (Krassovsky, 1972) is a complex quantity defined as the ratio of the relative amplitudes of the oscillations in the airglow emission rate and rotational temperature. So, the amplitude of the Krassovsky ratio, $|\eta|$, is given by:

$$|\eta| = \frac{\frac{\Delta E}{\overline{E}}}{\frac{\Delta T}{\overline{T}}},$$

where ΔE and ΔT are the wave amplitudes detected in the emission rate and in the rotational temperature, and $\overline{E}$ and $\overline{T}$ are the average emission rate and rotational temperature. The phase, ϕ, of Krassovsky's ratio is given by:

$$\phi = \phi_E - \phi_T,$$

where ϕ_E and ϕ_T are the phases of the respective oscillations in the emission rate and in the temperature, ϕ is positive when the emission rate oscillation leads the temperature oscillation.

Following the works of Hines and Tarasick (1987), Tarasick and Hines (1990) and Tarasick and Shepherd (1992a,b) the vertical wavelength, λ_z, of one perturbation can be determined from the complex value of the Krassovsky ratio by the expression:

$$\lambda_z \cong \frac{2\pi\gamma H}{(\gamma - 1)|\eta| \sin\phi},$$

where γ is the ratio of specific heats and H is the scale height. The Krassovsky ratios and the vertical wavelengths found for the semidiurnal tidal oscillation detected from our OH and O_2 data are listed in Tables 2 and 3, respectively.

For O_2 emission data $|\eta|$ values from 3.0 to 9.8 are found during the year, with 5.9 being the average value. A mean value of 6.9 is obtained from November to March and a mean value of 4.6 is obtained from April to September. For OH emission data greater values of $|\eta|$ are obtained throughout the year. A mean value of 8.6 is obtained from November to March when strong tidal signatures are present. Greater values are obtained from April to October when the monthly mean amplitudes are smaller than 3 K but those can not be considered very realiable. The phase of η is negative during the year, except during October for O_2 data (also during May and September for OH data), indicating an upward energy propagation in the O_2 layer throughout the year, except in October, and an upward energy propagation in the OH layer, except in May and September (although the small amplitudes detected in the OH temperature from May to September make this result subject to a large uncertainty).

The λ_z values from 18.5 km to 111.8 km are obtained for O_2 modulations. A mean value of 33.2 km is obtained from November to March and 56.9 km from April to September. Smaller values of λ_z are obtained from the OH data during the entire year. A mean value of 16.5 km is obtained for November to March and unrealistic small values are obtained from April to October, when the amplitudes of the tidal variations are the smallest.

Table 5. Amplitude growth factor. Values obtained from temperature amplitudes smaller than 3 K in bold.

	Temperature	Emission rate
Month	$g_{T_R} = \frac{\frac{\Delta T_{O_2}}{\overline{T}_{O_2}}}{\frac{\Delta T_{OH}}{\overline{T}_{OH}}}$	$g_{E_R} = \frac{\frac{\Delta I_{O_2}}{\overline{I}_{O_2}}}{\frac{\Delta I_{OH}}{\overline{I}_{OH}}}$
January	2.48	1.54
February	1.72	1.54
March	1.82	1.16
April	**2.02**	0.46
May	**5.00**	0.41
June	–	1.04
July	–	1.05
August	**7.77**	0.51
September	**1.93**	0.59
October	**1.34**	0.61
November	2.00	1.55
December	2.30	2.02

For the semidiurnal tide, vertical wavelengths of 36.4 km in the O_2 layer and of 27.7 km for the OH layer have been observed by Reisin and Scheer (1996). Values of 27.5 km in the O_2 layer and of 29 km in the OH layer have been deduced from observations taken in February at 37° N with a modulation of 15 h, and with extreme intensity variations of the O_2 atmospheric emission (Scheer and Reisin, 1998). In addition, vertical wavelengths from 12 to 76 km for waves of 3 to 9 h have been observed by Takahashi et al. (1999). Our observations agree with their results.

3.5 Equinox periods

The tidal modulation derived and listed in Table 4 reproduces the data numerically. The standard deviations after the fitting are very small and of similar magnitude during the entire year, however, larger standard deviations after the fitting seem to remain during October-November for both temperatures and emission rates and during April for both temperatures and the O_2 emission rate. These differences can be related to the change in the semidiurnal to diurnal character of the tide during early spring (March–April) and this could also be applied to September and October, although here we find that the semidiurnal tide is dominant during this period. These larger standard deviations after the fitting can be related to the presence of higher tidal harmonics, or greater wave activity. These differences could also be explained by the variations produced in the equinox transition periods. The equinox transition marks two significant periods in the annual variability of the mesosphere and lower thermosphere, marked by great activity in winter and more quiet activity period in summer. Shepherd et al. (1999) and Shepherd et al. (2004b) have discussed the observable effects in

the oxygen airglow during the spring and autumn transitions while Shepherd et al. (2002) and Shepherd et al. (2004a) have discussed the observable effects during the spring and autumn transition in the atmospheric temperature.

From the present work, the equinox periods could be characterized by:

1. Great changes in the phases of the tidal variations. These changes in the phases of the tidal activity during the months of September-October could be an indication of these transition periods (during March the phases of tidal activity show some changes but not as marked as during the September-October months).

2. During March-April and during September-October a small growth factor is detected for both temperature amplitudes and emission rate amplitudes, indicating a greater degree of dissipation than during the rest of the year (see Table 5).

3. The fact that large standard deviations after the fitting are obtained for October–November, in both temperatures and emission rates, and somewhat larger standard deviations after the fitting are present for April, in both temperatures and O_2 emission rates, than during the rest of the year, can be connected to the presence of higher tidal harmonic and wave activity and also with the changes that are produced due to the equinox transitions during these periods.

4 Conclusions

The monthly mean diurnal variations for temperatures and emission rates, deduced from the OH(6-2) Meinel and O_2(0-1) atmospheric bands at a latitude of 37.06° N, from SATI operation in 1998 to 2003, have been presented. A clear daily modulation is found in temperatures and emission rates:

– The modulation is predominantly semidiurnal in both temperatures and emission rates throughout the year.

– During spring the semidiurnal variation changes to a diurnal type, in both temperature and emission rates.

– During late autumn and early winter OH emission rates show both diurnal and semidiurnal modulations.

From summer to late autumn the amplitudes of the diurnal variation decrease by more than a factor of two compared with those in winter and spring.

Mean vertical wavelengths for the semidiurnal modulation of 33.2 km in the O_2 layer and of 16.5 km for the OH layer are obtained from November to March with our data.

A clear upward energy propagation is observed during most of the year, with some indication of possible downward energy propagation close to the equinoxes.

Both emission rates and rotational temperatures present a similar pattern of diurnal variation throughout the year, yielding maximum values some time after midnight.

It is clear that, in general, T_{O_2} leads the O_2 emission rates, that O_2 rotational temperatures also lead the OH rotational temperatures and that T_{OH} leads the OH emission rates. Both emission rates have phase shifts from about 3 h to 7 h (-5 h) for the entire year, with the O_2 emission rate leading the OH emission rate, expect in July, August and September, when the OH emission rate leads the O_2 emission rate.

Acknowledgement. This research was partially supported by the Dirección General de Investigación (DGI) under projects AYA2000-1559 and AYA2003-04651, the Comisión Interministerial de Ciencia y Tecnología under projects REN2001-3249 and ESP2004–01556, the Junta de Andalucía, NATO under a Collaborative Linkage Grants 977354 and 979480 and INTAS under the research project 03-51-6425. We very gratefully acknowledge the staff of Sierra Nevada Observatory for their help and assistance with the SATI instrument. We wish to thank the referee for useful comments and suggestions.

Topical Editor U. P. Hoppe thanks a referee for his/her help in evaluating this paper.

References

Abreu, V. J. and Yee, J. H.: Diurnal and seasonal variation of the nighttime OH(8-3) emission at low latitudes, J. Geophys. Res., 94, 11 949–11 957, 1989.

Burrage, M. D., Arvin, N., Skinner, W. R., and Hays, P. B.: Observations of the O_2 atmospheric band nightglow by the High Resolution Doppler Imager, J. Geophys. Res., 99, 15 017–15 023, 1994.

Burrage, M. D., Wu, D. L., Skinner, W. R., Ortland, D. A., and Hays, P. B.: Latitude and seasonal dependence of the semidiurnal tide observed by the high-resolution Doppler imager, J. Geophys. Res., 100, 11 313–11 321, 1995.

Crary, J. D. and Forbes, J. M.: On the extraction of tidal information from measurements covering a fraction of a day, Geophys. Res. Lett., 10, 580–582, 1983.

Chapman, S. and Lindzen, R. S.: Atmospheric tides: thermal and gravitational, Gordon and Breach, New York, 1–23, 1970.

Choi, G. H., Monson, I. K., Wickwar, V. B., and Rees, D.: Seasonal and diurnal variations of wind and temperature near the mesopause from Fabry-Perot interferometer observations of OH Meinel emissions, Adv. Space Res., 21, 847–850, 1998.

Forbes, J. M., Portnyagin, Yu. I., Skinner, W., Vincent, R. A., Solovjova, T., Merzlyakov, E., Nakamura, T., and Palo, S.: Climatological lower thermosphere winds as seen by ground-based and space-based instruments, Ann. Geophys., 22, 1931–1945, 2004,
SRef-ID: 1432-0576/ag/2004-22-1931.

Hagan, M. E., Burrage, M. D., Forbes, J. M., Hackney, J., Randel, W. J., and Zhang, X.: GSWM-98: Results for migrating solar tides, J. Geophys. Res., 104, 6813–6828, 1999.

Hines, C. O. and Tarasick, D. W.: On the detection and utilization of gravity waves in airglow studies, Planet. Space Sci., 35, 851–866, 1987.

Jacobi, Ch., Portnyagin, Yu. I., Solovjova, T. V., Hoffmann, P., Singer, W., Fahrutdinova, A. N., Ishmuratov, R. A., Beard, A. G., Mitchell, N. J., Muller, H. G., Schminder, R., Kürschner, D., Manson, A. H., and Meek, C. E.: Climatology of the semidiurnal tide at 52–56 N from ground-based radar wind measurements 1985–1995, J. Atmos. Solar-Terr. Phys., 61, 975–991, 1999.

Krassovsky, V. I.: Infrasonic variations of OH emission in the upper atmosphere, Ann. Geophys., 28, 739–746, 1972.

Liu, A. Z. and Swenson, G. R.: A modeling study of O_2 and OH airglow perturbations induced by atmospheric gravity waves, J. Geophys. Res., 108(D4), 4151, doi:10.1029/2002JD2474, 2003.

López-González, M. J., Murtagh, D. P., Espy, P. J., López-Moreno, J. J., Rodrigo, R., and Witt, G.: A model study of the temporal behaviour of the emission intensity and rotational temperature of the OH Meinel bands for high-latitude summer conditions, Ann. Geophys., 14, 59–67, 1996,
SRef-ID: 1432-0576/ag/1996-14-59.

López-González, M. J., Rodríguez, E., Wiens, R. H., Shepherd, G. G., Sargoytchev, S., Brown, S., Shepherd, M. G., Aushev, V. M., López-Moreno, J. J., Rodrigo, R., and Cho, Y.-M.: Seasonal variations of O_2 Atmospheric and OH(6-2) airglow and temperature at mid-latitudes from SATI observations, Ann. Geophys., 22, 819–828, 2004,
SRef-ID: 1432-0576/ag/2004-22-819.

Manson, A. H., Meek, C. E., Chshyolkova, T., Avery, S. K., Thorsen, D., MacDougall, J. W., Hocking, W., Murayama, Y., Igarashi, K., Namboothiri, S. P., and Kishore, P.: Longitudinal and latitudinal variations in dynamic characteristics of the MLT (70–95 km): a study involving the CUJO network, Ann. Geophys., 22, 347–365, 2004,
SRef-ID: 1432-0576/ag/2004-22-347.

Pancheva, D., Mukhtarov, P., Mitchell, N. J., Beard, A. G., and Muller, H. G.: A comparative study of winds and tidal variability in the mesosphere/lower-thermosphere region over Bulgaria and the UK, Ann. Geophys., 18, 1304–1315, 2000,
SRef-ID: 1432-0576/ag/2000-18-1304.

Pancheva, D., Merzlyakov, E., Mitchell, N. J., Portnyagin, Yu., Manson, A. H., Jacobi, Ch., Meek, C. E., Luo, Y., Clark, R. R., Hocking, W. K., MacDougall, J., Muller, H. G., Kürschner, D., Jones, G. O. L., Vincent, R. A., Reid, I. M., Singer, W., Igarashi, K., Fraser, G. I., Fahrutdinova, A. N., Stepanov, A. M., Poole, L. M. G., Malinga, S. B., Kashcheyev, B. L., and Oleynikov, A. N.: Global-scale tidal variability during the PSMOS campaign of June–August 1999: interaction with planetary waves, J. Atmos. Solar-Terr. Phys., 64, 1865–1896, 2002.

Pendleton Jr., W. R. and Taylor, M. J.: The impact of L-uncoupling on Einstein coefficients for the OH Meinel (6,2) band: implications for Q-branch rotational temperatures, J. Atmos. Solar-Terr. Phys., 64, 971–983, 2002.

Petitdidier, M. and Teitelbaum, H.: Lower thermosphere emissions and tides, Planet. Space Sci., 25, 711–721, 1977.

Portnyagin, Y. I., Solovjova, T. V., Makarov, N. A., Merzlyakov, E. G., Manson, A. H., Meek, C. E., Hocking, W., Mitchell, N., Pancheva, D., Hoffmann, P., Singer, W., Murayama, Y., Igarashi, K., Forbes, J. M., Palo, S., Hall, C., and Nozawa, S.: Monthly mean climatology of the prevailing winds and tides in the Arctic mesosphere/lower thermosphere, Ann. Geophys., 22, 3395–3410, 2004,
SRef-ID: 1432-0576/ag/2004-22-3395.

Reisin, E. R. and Scheer, J.: Characteristics of atmospheric waves in the tidal period range derived from zenith observations of O_2(0-1) Atmospheric and OH(6-2) airglow at lower midlatitudes, J. Geophys. Res., 101, 21 223–21 232, 1996.

Riggin, D. M., Meyer, C. K., Fritts, D. C., Jarvis, M. J., Murayama, Y., Singer, W., Vincent, R. A., and Murphy, D. J.: MF radar observations of seasonal variability of semidiurnal motions in the mesosphere at high northern and southern latitudes, J. Atmos. Solar-Terr. Phys., 65, 483–493, 2003.

Sargoytchev, S., Brown, S., Solheim, B. H., Cho, Y.-M., Shepherd, G. G., and López-González, M. J.: Spectral airglow temperature imager (SATI) – a ground based instrument for temperature monitoring of the mesosphere region, Appl. Opt., 43, 5712–5721, 2004.

Scheer, J. and Reisin, E. R.: Rotational temperatures for OH and O_2 airglow bands measured simultaneously from El Leoncito (31°48′ S), J. Atmos. Terr. Phys., 52, 47–57, 1990.

Scheer, J. and Reisin, E. R.: Extreme intensity variations of O_2b airglow induced by tidal oscillations, Adv. Space Res., 21, 827–830, 1998.

Shepherd, M. G. and Fricke-Begemann, C.: Study of the tidal variations in mesospheric temperature at low and mid latitudes from WINDII and potassium lidar observations, Ann. Geophys., 22, 1513–1528, 2004,
SRef-ID: 1432-0576/ag/2004-22-1513.

Shepherd, G. G., McLandress, C., and Solheim, B. H.: Tidal influence on O(^{1}S) airglow emission rate distributions at the geographic equator as observed by WINDII, Geophys. Res. Lett., 22, 275–278, 1995.

Shepherd, G. G., Roble, R. G., Zhang, S. P., McLandress, C., and Wiens, R. H.: Tidal influences on midlatitude airglow: Comparison of satellite and ground-based observations with TIME-GCM predictions, J. Geophys. Res., 103, 14 741–14 751, 1998.

Shepherd, G. G., Stegman, J., Espy, P., McLandress, C., Thuillier, G., and Wiens, R. H.: Springtime transition in lower thermospheric atomic oxygen, J. Geophys. Res., 104, 213–223, 1999.

Shepherd, M. G., Espy, P. J., She, C. Y., Hocking, W., Keckhut, P., Gavrilyeva, G., Shepherd, G. G., and Naujokat, B.: Springtime transition in upper mesospheric temperature in the Northern Hemisphere, J. Atmos. Solar-Terr. Phys., 64, 1183–1199, 2002.

Shepherd, M. G., Rochon, Y. I., Offermann, D., Donner, M., and Espy, P. J.: Longitudinal variability of mesospheric temperatures during equinox at middle and high latitudes, J. Atmos. Solar-Terr. Phys., 66, 463–479, 2004a.

Shepherd, G. G., Stegman, J., Singer, W., and Roble, R. G.: Equinox transition in wind and airglow observations, J. Atmos. Solar-Terr. Phys., 66, 481–491, 2004b.

Takahashi, H., Sahai, Y., Clemesha, B. R., Batista, P. P., and Teixeira, N. R.: Diurnal and seasonal variations of the OH (8,3) airglow band and its correlation with OI 5577, Planet. Space Sci., 25, 541–547, 1977.

Takahashi, H., Gobbi, D., Batista, P. P., Melo, S. M. L., Teixeira, N. R., and Buriti, R. A.: Dynamical influence on the equatorial airglow observed from the South American sector, Adv. Space Res., 21, 817–825, 1998.

Takahashi, H., Batista, P. P., Buriti, R. A, Gobbi, D., Nakamura, T. Tsuda, T., and Fukao, S.: Response of the airglow OH emission, temperature and mesopause wind to the atmospheric wave propagation over Shigaraki, Japan, Earth Planets Space, 51, 863–875, 1999.

Tarasick, D. W. and Hines, C. O.: The observable effects of gravity waves on airglow emissions, Planet. Space Sci., 38, 1105–1119, 1990.

Tarasick, D. W. and Shepherd, G. G.: Effects of gravity waves on complex airglow chemistries. 1 $O_2(b^1\Sigma_g^+)$ emission, J. Geophys. Res., 97, 3185–3193, 1992a.

Tarasick, D. W. and Shepherd, G. G.: Effects of gravity waves on complex airglow chemistries. 2. OH emission, J. Geophys. Res., 97, 3195–3208, 1992b.

Wiens, R. H. and Weill, G.: Diurnal, annual and solar cycle variations of hydroxyl and sodium nightglow intensities in the

Europe-Africa sector, Planet. Space Sci., 21, 1011–1027, 1973.
Wiens, R. H., Zhang, S. P., Peterson, R. N., and Shepherd, G. G.: MORTI: A Mesopause Oxygen Rotational Temperature Imager, Planet. Space Sci., 39, 1363–1375, 1991.
Wiens, R. H., Zhang, S. P., Peterson, R. N., and Shepherd, G. G.: Tides in emission rate and temperature from O_2 nightglow over Bear Lake Observatory, Geophys. Res. Lett., 22, 2637–2640, 1995.
Wiens, R. H., Moise, A., Brown, S., Sargoytchev, S., Peterson, R. N., Shepherd, G. G., López-González, M. J., López-Moreno, J. J., and Rodrigo, R.: SATI: A Spectral Airglow Temperature Imager, Adv. Space Res., 19, 677–680, 1997.
Zhang, S. P. and Shepherd, G. G.: The influence of the diurnal tide on the $O(^1S)$ and OH emission rates observed by WINDII on UARS, Geophys. Res. Lett., 26, 529–532, 1999.
Zhang, S. P., Shepherd, G. G., and Roble, R. G.: Tidal influence on the oxygen and hydroxyl nightglows: Wind Imaging Interferometer observations and thermosphere/ionosphere/mesosphere electrodynamics general circulation model, J. Geophys. Res., 106, 21 381–21 393, 2001.